

Synthesis of MgFe₂O₄-TiO₂-SiO₂ Ternary Nanocomposite: Synthesis, Characterization and Photocatalytic Degradation of Brilliant Green dye

M. SUNEETHA^{1,✉}, G. HIMA BINDU^{1,*}, K. JYOTHI PRIYA^{1,✉}, CH. RAMYA KUMARI^{1,✉},
G. SUPRIYA^{1,✉}, D. SWAPNA^{1,2,✉} and S. PAUL DOUGLAS^{1,*}

¹Department of Engineering Chemistry, AU College of Engineering, Andhra University, Visakhapatnam-530003, India

²Department of Chemistry, Dadi Institute of Engineering and Technology, Anakapalli-531002, India

*Corresponding authors: E-mail: himabinduauce@gmail.com; pauldouglas12@gmail.com

Received: 27 September 2024;

Accepted: 21 December 2024;

Published online: 31 January 2025;

AJC-21882

Wet chemical techniques were used to synthesize magnetic nanocomposites effectively, whereas the sol-gel process was used to individually prepare the magnetic nanocomposites. The UV-DRS, FTIR, SEM, EDS, TEM, XRD and VSM methods were used to characterize the MgFe₂O₄-TiO₂-SiO₂ nanocomposite. The photocatalytic activity of the nanocomposite as a photocatalyst towards the degradation of Brilliant green was studied under visible light irradiation. The photocatalytic activity showed that the nanocomposites were still effective after three cycles of catalysis and degraded brilliant green dye at a rate of 100%. The structural, morphological and optical properties of the composites have been investigated by X-ray diffraction and high-resolution transmission electron microscopy (HR-TEM) techniques. The HR-TEM images confirm the formation of ternary nanocomposites having smaller particle sizes, whereas the surface morphology of nanocomposite was examined by SEM and EDS techniques. In UV-DRS analysis, the band gap energy value of the nanocomposite was found to be 2.3 eV. These results concluded that a synthesized photocatalyst is effective, reusable, easily separable, low-cost and eco-friendly. The antibacterial activity of the prepared nanocomposites was also evaluated against Gram-negative *Escherichia coli* and Gram-positive *Staphylococcus aureus* bacteria. The novel nanocomposites have shown efficient photocatalytic activity and better antibacterial activity.

Keywords: MgFe₂O₄/TiO₂/SiO₂, Photocatalytic activity, Nanocomposite, Brilliant green, Sol-gel method, Antibacterial activity.

INTRODUCTION

The explosive growth in population today is driving accelerated industrialization in sectors such as paper, textile, leather and cosmetics. These industries use colours of their products with a variety of synthetic organic dyes [1]. These product colour emissions contaminate the environment, mostly in the water stream, which results in a shortage of drinking water and harms human health [2]. Dyes are the synthetic organic compounds that come in various types, such as acidic, basic, sulfur, nitro triphenylmethane and azo dyes. Brilliant green (BG), a triphenylmethane-based dye, is widely used in the leather, textile and biological industries. However, water contaminated with brilliant green poses serious health risks to humans, potentially causing hypertension and issues related to the heart, kidneys and lungs. It may even have carcinogenic effects on living organisms [3].

The photocatalysis process is widely considered to be among the most effective methods for eliminating organic pollutants from wastewater [4]. In the presence of sunlight, organic contaminants undergo breakdown through a process involving photocatalysis. Sunlight and catalysts generate free radicals, which then engage with the pollutants, leading to their decomposition. Nanoscale materials, utilized as catalysts, can enhance efficiency by 100% relative to bulk materials due to their high surface area to volume ratios [5]. The semiconductor materials having wide band gap exhibit great stability and photocatalytic activity [6]. TiO₂ is one of the best semiconductor materials that has been employed in photocatalysis among other semiconductors because of its wide band gap (3.2 eV), excellent electrical properties and optical properties, high chemical and photostability, strong photocatalytic activity, low cost, nontoxic nature and ecological [7]. TiO₂ absorbs only UV photons (wavelengths shorter than 400 nm), accounting for approximately 5% of solar

light, which significantly restricts its application. Semiconductor metal oxides are combined with TiO_2 to boost its photocatalytic capacity, leading to the successful formation of heterojunctions that improve the photocatalytic performance of TiO_2 under visible light and near-infrared region [8]. Moreover, TiO_2 may combine in an extremely favourable way with a semiconductor that has a reduced band gap to produce TiO_2 -based materials with magnetic properties [9].

Magnesium ferrite, characterized by its small band gap of 2.1 eV, is a semiconductor with a spinel structure capable of absorbing visible light [10]. Magnesium ferrite is effective for removing arsenic and has a high adsorption capacity. It is inexpensive, stable and safe for biological tissues also [11]. The previously described properties of MgFe_2O_4 are combined with TiO_2 to increase surface area, inhibit photogenerated charge carrier recombination and modify the band gap to expand into visible [12]. Due to the small size of TiO_2 particles, separating and recovering suspended nano-titania from treated water is extremely challenging, owing to the superior proximity of metal oxides to pollutants and their accessibility as a catalytic surface [13]. It also appears that the silica layer stopped the iron oxide from serving as a centre for electron-hole recombination. Further, this results in increased photoactivity [14]. Because to their great mechanical strength, broad surface area, low toxicity, biodegradability and sustainability, they are also the best adsorbents for removing heavy metal ions (As, Pd) from water [15]. And $\text{TiO}_2/\text{SiO}_2$ both acts as additive properties (Ti-O-Si) bond activates the catalytic centers of composite oxide in oxidation reactions of organic compound. Electron hole-pair on $\text{SiO}_2\text{-TiO}_2$ leads to increase photocatalytic activity and self-cleaning features (hydrophobic) [16]. The preparation and characterization of MgFe_2O_4 as a source of iron ions (a dopant) coated with anatase titanium nanoparticles (a photocatalytic component) and SiO_2 (adsorbent) using the sol-gel method is the aim of this work. By adding an external magnetic field, the magnetic composite photocatalyst can be both recovered and fluidized. Utilizing UV and solar radiation to degrade Brilliant green dye, the magnetic photocatalyst was examined using UV-DRS, SEM-EDS, TEM, XRD, FTIR and VSM techniques.

EXPERIMENTAL

All the chemicals and reagents *viz.* tetraethyl orthosilicate, ethylene glycol, magnesium nitrate, ferric citrate, citric acid, titanium tetrachloride, hydrochloric acid, ammonia and ethanol were of analytical grade and utilized without further purification. All the reactions were performed using deionized water.

Characterization: The synthesized materials were characterized using a variety of approaches. The crystallite size and purity of the prepared photocatalyst were measured through X-ray diffraction (XRD) using a Bruker DX-5 Advanced with a proportional counter and $\text{CuK}\alpha$ radiation ($\lambda = 1.54 \text{ \AA}$). Scanning electron microscopy (SEM) images were collected using a Carl Zeiss Gemini 300 from Germany and transmission electron microscopy (TEM) was utilized to establish the form and particle size of the nanocomposite. The key vibrations of the functional groups of the nanocomposite were observed using Fourier transform infrared (FTIR) spectroscopy on IR Prestige

21 in the range of $4000\text{-}500 \text{ cm}^{-1}$. UV-DRS was utilized to investigate the structure and band gap, utilizing a Shimadzu 2600R and BaSO_4 as a reference in the range of 200-800 nm. The magnetic characteristics of the photocatalyst nanocomposite were measured using a vibrating sample magnetometer (VSM) throughout a temperature range.

Synthesis of SiO_2 : Tetraethyl orthosilicate (TEOS) was added to 0.3 mol of ethanol followed by the addition of 0.1 to 0.75 mol ammonia and 0.25-2.0 mol of ethanol. Stirred the solution mixed vigorously for 0.5 h, dried at $80 \text{ }^\circ\text{C}$ for 6 h and then calcined at $900 \text{ }^\circ\text{C}$ for 2 h.

Synthesis of TiO_2 : TiCl_4 (6.9 g) was added slowly to 350 mL of distilled water containing 0.5 mL of HCl solution in a beaker covered with aluminum foil. A white, curdy precipitate was formed when the beaker was stirred kept on magnetically for 1 h and then heated at $80\text{-}100 \text{ }^\circ\text{C}$ on a hot plate. The fine powder was obtained and kept in a hot air oven at $80 \text{ }^\circ\text{C}$ to evaporate the moisture. The powder was finally ground in a motor pestle and calcined at $400 \text{ }^\circ\text{C}$ for 2 h [17].

Synthesis of MgFe_2O_4 : Magnesium nitrate (4.23 g) dissolved in 10 mL of distilled water was added to an aqueous solution of ferric citrate (71.64 g) followed by the addition of 12.6 g of citric acid and then adjusted the pH of the solution to neutral by adding few ammonia slowly and then 20 mL of ethylene glycol. After 2 h of heating on a hot plate, the solution was reduced to a dry powder. After calcination at $800 \text{ }^\circ\text{C}$ to form fine magnesium ferrite nanopowder.

Synthesis of $\text{MgFe}_2\text{O}_4/\text{TiO}_2/\text{SiO}_2$ nanocomposites: To enable investigation of the effect of TiO_2 loading on SiO_2 and further, these are loadings on magnesium ferrite nanocomposite at 0.1, 0.1 and 0.8 g, respectively. TiO_2 (0.1 g) was placed into a motor followed by the addition of 0.1 g of SiO_2 and 0.8 g of MgFe_2O_4 powder and then grounded using pestle to obtain finely $\text{MgFe}_2\text{O}_4\text{-TiO}_2\text{-SiO}_2$ nanocomposite.

RESULTS AND DISCUSSION

XRD studies: Fig. 1 shows the X-ray diffraction patterns of $\text{MgFe}_2\text{O}_4\text{-TiO}_2\text{-SiO}_2$ photocatalytic nanocomposite. The diffraction peaks at 2θ values of 25° , 30° , 35° , 55° and 57° corresponding to the planes (101) (220) (311) (105) (333), respectively. Indexing using JCPDS card no. 73-1720, the peaks observed at 30° , 36° , 57° correspond to plane (220) (311) (333) indicate that MgFe_2O_4 is the primary phase and also highlighted the crystalline nature of the sample. The SiO_2 peak is absent due to its amorphous nature, while the peaks corresponding to TiO_2 are observed at 2θ values based on JCPDS card No. 21-1272, with prominent peaks at 25° and 55° , associated with the (101) and (105) planes. These results indicate that the composite sample was successfully formed, with MgFe_2O_4 exhibiting a crystalline structure, while TiO_2 exists in the anatase phase, consistent with recent reports [18,19].

UV-DRS studies: The Tauc plot nanocomposite was employed to ascertain the correlation of E_g with the indirect band gap energy of $\text{MgFe}_2\text{O}_4\text{-TiO}_2\text{-SiO}_2$, which was estimated using UV-DRS spectrum within the region of 200-800 nm for the prepared nanocomposite (Fig. 2). The characteristic band appears at 440 nm.

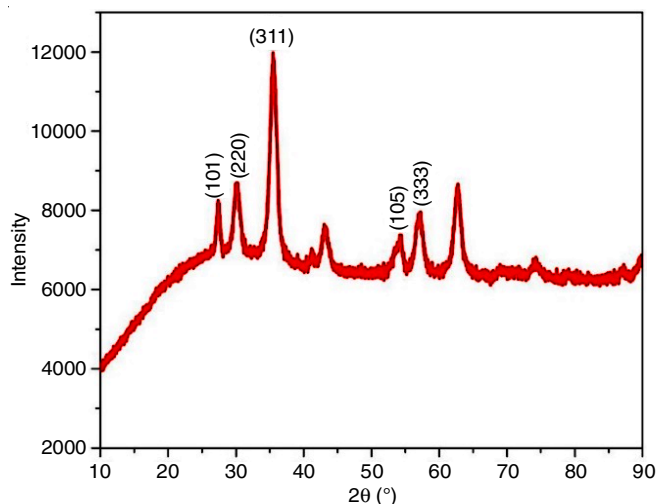


Fig. 1. XRD pattern of MgFe₂O₄/TiO₂/SiO₂ ternary nanocomposite

$$\text{Energy band gap} = E_g = hv = \frac{hc}{\lambda}$$

The optical band gap for SiO₂ nanoparticles was evaluated using the following equation:

$$(\alpha hv)^n = A(hv - E_g)$$

The nanocomposite exhibits an indirect band gap (E_g) of 2.29 eV and a maximum absorption wavelength at 440 nm. The efficiency of photocatalytic activity is significantly determined by the electronic band gap energy. For a photocatalyst to be efficient, it must possess a band gap of less than 3.0 eV, allowing for enhanced light absorption within the visible spectrum and improving the utilization of solar energy [20]. The band gap between 1.5 and 2.4 eV has the potential for photocatalytic water splitting, thus, nanocomposites are a good photocatalyst for air and water purification.

SEM and EDAX: MgFe₂O₄-TiO₂-SiO₂ is heterogeneous with high degree of smooth on the surface observed. Based on the SEM image (Fig. 3a) at low magnification, it is observed

that structure seems to consist of aggregated particles, forming agglomeration. Whereas Fig. 3b-c focuses more closely on the individual particles, possibly revealing finer details such as the crystalline appearance of the material. The particle size distribution based on histogram curve (Fig. 3d) suggests a normal or Gaussian distribution, with an average particle size of approximately 38.03 nm. The EDS spectrum (Fig. 3e) and elemental composition exhibit the presence of 56.4% Fe, 31.6% O, 1.5% Ti, 2.5% Si and 8.0% Mg which confirm the formation of pure MgFe₂O₄-TiO₂-SiO₂ nanocomposite.

TEM studies: Fig. 4a illustrates the structure of small particles which further confirms the nanoparticles. The darker regions likely represent agglomerated or more dense particles, while the lighter areas suggest lower electron density or smaller particles. The TEM images (Fig. 4b-c) shows a mixture of small particles and larger spherical structures, which provides an overall view of the particle distribution, emphasizing the bulk morphology of the sample. The selected area electron diffraction (SAED) pattern (Fig. 4d) consists of bright spots arranged in a regular manner, which indicates that the material is crystalline. The distances between spots (labeled as 5.17 nm) correspond to the specific interplanar spacings, which can be used to identify the crystallographic structure of the material.

FT-IR studies: The FTIR spectrum of MgFe₂O₄-TiO₂-SiO₂ nanocomposite particles is shown in Fig. 5. The major peaks appear at 3853, 3408, 1501, 1103, 700-400 cm⁻¹. The absorption bands 3408, 3853 cm⁻¹ are the stretching mode of O-H groups on surface (M-O bond strength) of photocatalyst. This is significant as it improves the photocatalytic activity of TiO₂ by increasing its capacity to absorb oxygen. The absorption peak appear at 1501 cm⁻¹ is O-H bending vibration. The absorption band observed at 469 cm⁻¹ corresponds to the stretching vibrations of Fe-O bonds, thereby confirmed the presence of metal oxides, such as iron oxide. The peak at 487 cm⁻¹ is due to the stretching vibrations of Ti-O in anatase TiO₂. However, a band observed at 1103 cm⁻¹ correspond to the Si-O-Si stretching vibrations in the FTIR spectrum is confirmed.

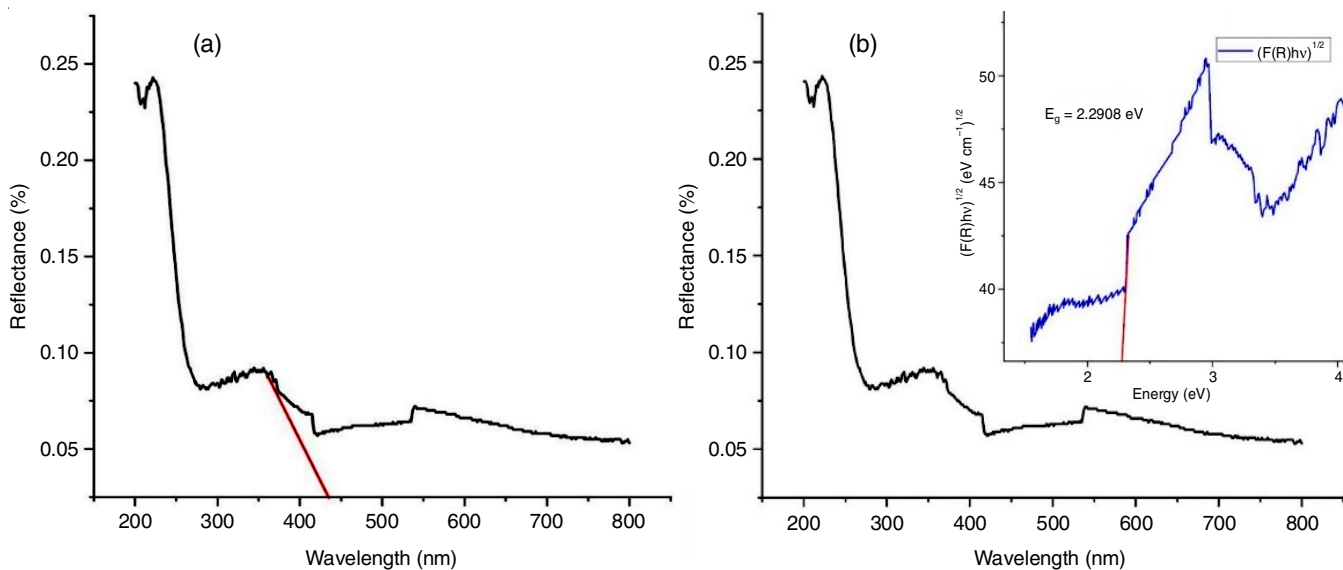


Fig. 2. (a) UV-visible absorption spectra and (b) band gap energy of MgFe₂O₄/TiO₂/SiO₂ ternary nanocomposite

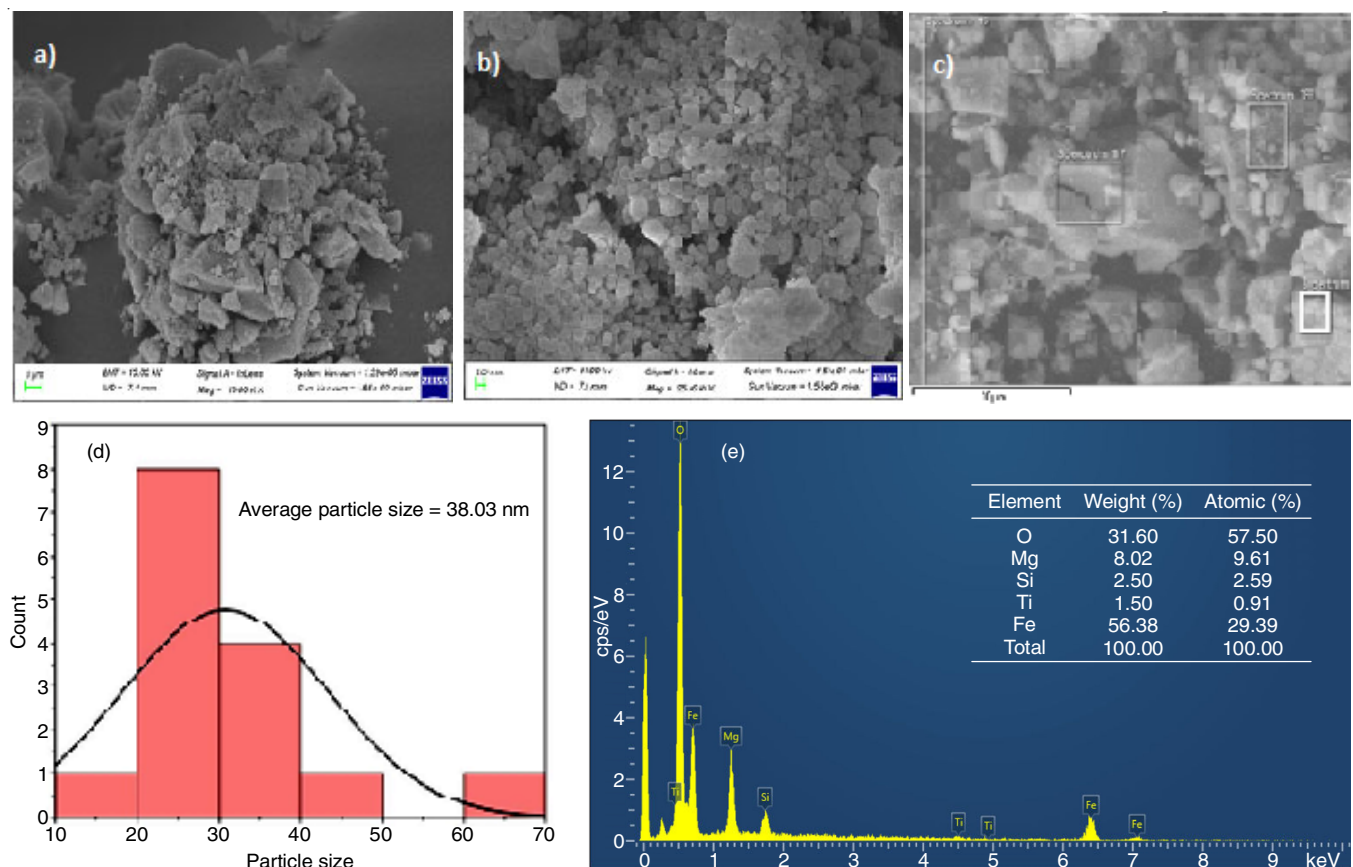


Fig. 3. SEM images (a) 1 μm (b) 10 nm (c) 100 nm (d) average particle size histogram and (e) EADX image of MgFe₂O₄/TiO₂/SiO₂ nanocomposite

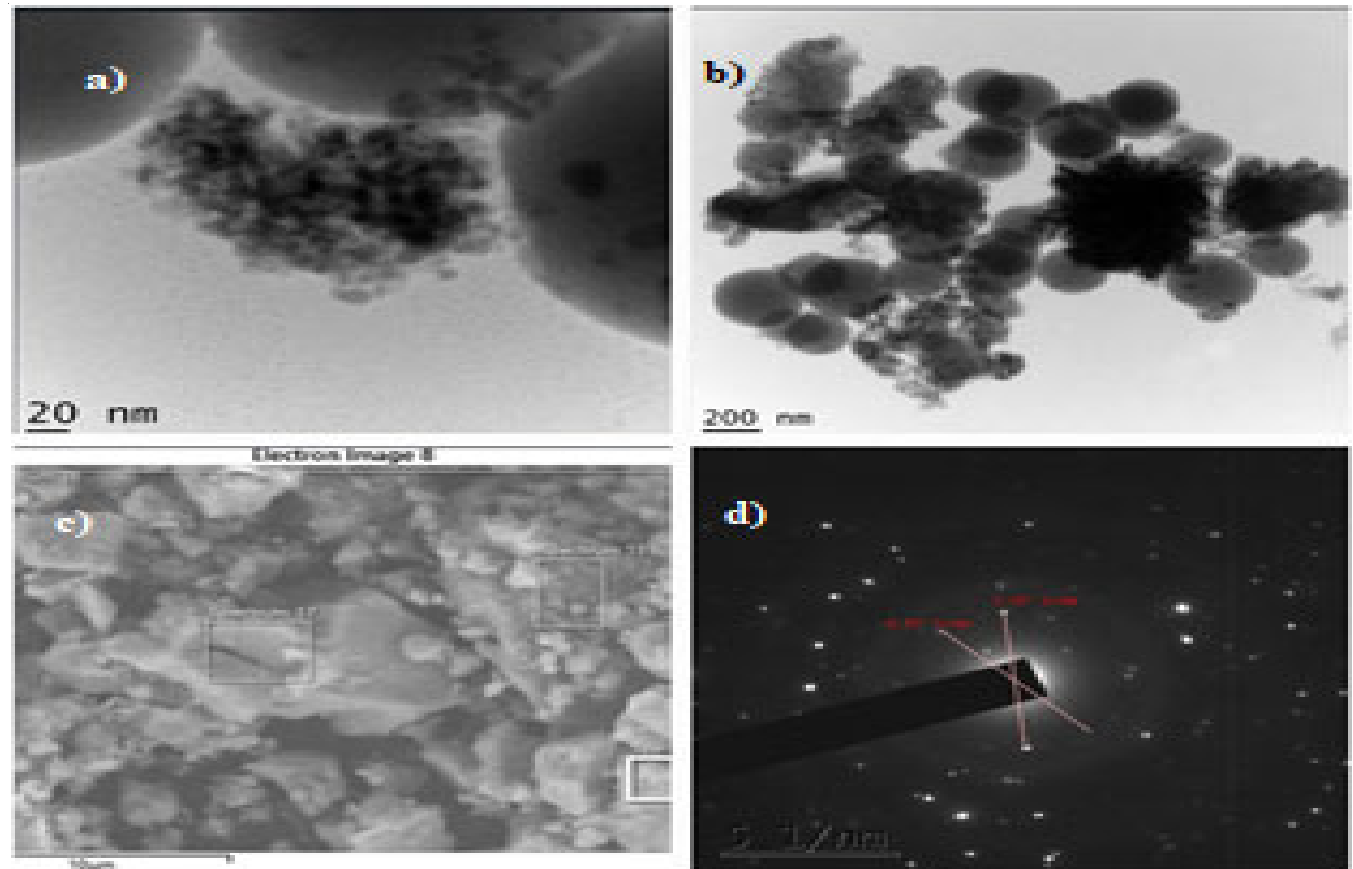


Fig. 4. (a) 20 nm (b) 200 nm (c) 100 nm TEM images of MgFe₂O₄/TiO₂/SiO₂, (d) SAED pattern of MgFe₂O₄/TiO₂/SiO₂ ternary nanocomposite

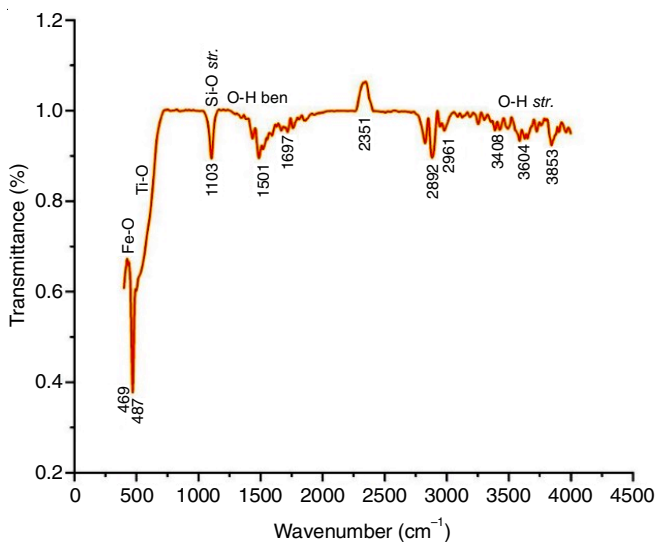


Fig. 5. FTIR spectrum of $\text{MgFe}_2\text{O}_4/\text{TiO}_2/\text{SiO}_2$ ternary nanocomposite

Magnetic properties: The magnetic properties were examined using a vibrating sample magnetometer (VSM) at room temperature. The magnetic behaviour of the prepared nanocomposite is important to its application as a regenerable and reusable magnetic heterogeneous catalyst. Magnesium ferrite nanoparticles show the superparamagnetic behaviour, with a saturation magnetization of 60 emu/g and nearly zero coercivity (Fig. 6). The prepared $\text{MgFe}_2\text{O}_4/\text{TiO}_2/\text{SiO}_2$ nanocomposite exhibits superparamagnetic behaviour, with a saturation magnetization of 32.5 emu/g and coercivity around zero. The magnetization is lower due to the presence of metal oxides. Thus, this nanocomposite is suitable for reusable magnetic separation application of photocatalytic particles.

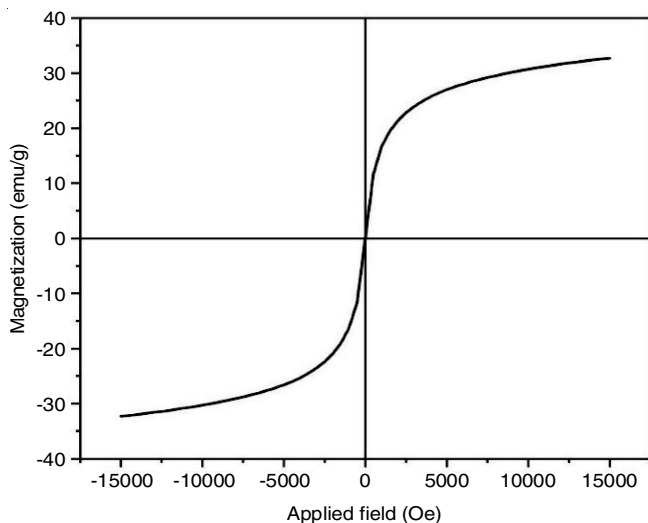


Fig. 6. Magnetization loop for $\text{MgFe}_2\text{O}_4/\text{TiO}_2/\text{SiO}_2$ composite at room temperature

UV-visible studies: The UV-visible spectrum for brilliant green in aqueous solution were observed, revealing a high-intensity peak at the absorption wavelength, $\lambda_{\text{max}} = 625$ nm, in the visible range. The percentage of degradation of brilliant green was examined at various time intervals.

Photocatalytic degradation of brilliant green dye: The photocatalytic activity of the prepared nanocomposites was assessed by measuring the degradation of brilliant green dye under visible light irradiation. Initially, MgFe_2O_4 (without TiO_2) did not affect the photodegradation of aqueous brilliant green dye solution. However, using $\text{MgFe}_2\text{O}_4/\text{TiO}_2/\text{SiO}_2$ nanocomposite as photocatalyst, degraded the brilliant green dye efficiently. However, the optimized parameters such as pH, catalyst dosage, dye degradation and temperature influence must be evaluated in order to obtain the efficiency of photocatalyst.

Initial dye concentration: By adjusting the initial brilliant green dye concentration from 5 to 100 ppm at fixed pH = 8 and catalyst loading of 10 mg/L, the impact of initial brilliant green dye concentration on the photocatalytic performance of $\text{MgFe}_2\text{O}_4/\text{TiO}_2/\text{SiO}_2$ composite was investigated. Fig. 7 shows that using 10 mg/L of brilliant green dye concentration, the maximal degradation rate (100%) was reached in 125 min. The reduction in the degradation rate as the concentration of brilliant green dye increases can be attributed to the blanket effect, where brilliant green dye molecules cover the active sites on the catalyst surface, thereby limiting the generation of OH radicals. Although the catalyst dosage was kept constant at 10 mg/L, a proportional number of reactive species could not be generated due to the increasing quantity of brilliant green dye molecules. The efficiency of brilliant green dye molecules to block visible light is an additional factor influencing the reduction in the degradation rate. Thus, the results demonstrated that 10 ppm of $\text{MgFe}_2\text{O}_4/\text{TiO}_2/\text{SiO}_2$ is an a potent photocatalyst for the breakdown of brilliant green dye solution (10 ppm).

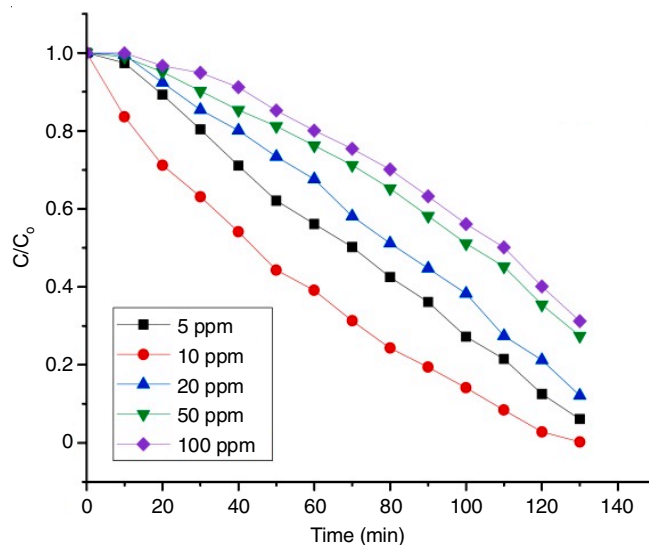


Fig. 7. Effect of dye concentration on $\text{MgFe}_2\text{O}_4/\text{TiO}_2/\text{SiO}_2$

Effect of pH: The pH of the solution containing $\text{MgFe}_2\text{O}_4/\text{TiO}_2/\text{SiO}_2$ nanocomposite was increased from 4 to 8 by adding 0.1 M HCl/NaOH solution to the solution. 500 mg of $\text{MgFe}_2\text{O}_4/\text{TiO}_2/\text{SiO}_2$ nanocomposite is added to an aqueous solution containing Brilliant green dye and the pH was measured and found to be 4.0. The dye degradation at different pH values showed that after 100 min of radiation pH 8 has shown 100% dye degradation as shown in Fig. 8. As the pH was increased

to 8, the degradation percentage initially increased and then gradually decreased. At lower pH levels, the catalyst surface becomes negatively charged.

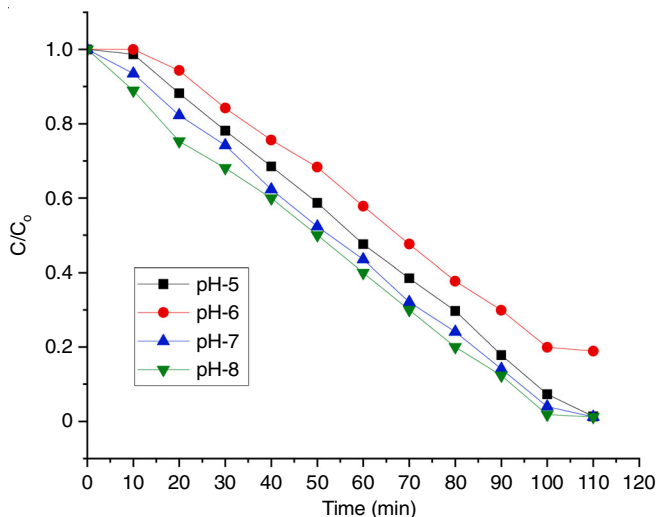


Fig. 8. Effect of pH on $\text{MgFe}_2\text{O}_4/\text{TiO}_2/\text{SiO}_2$

Effect of temperature: Increasing the temperature from 25 to 40 °C and the photocatalytic efficiency can be increased by approximately two to three times. The results demonstrated that the molecules cannot be pyrolyzed by heating to a temperature below 40 °C or self-degraded by absorbing radiation. The effective degradation was achieved when both $\text{MgFe}_2\text{O}_4/\text{SiO}_2/\text{TiO}_2$ and UV radiation were applied (Fig. 9) indicating that $\text{MgFe}_2\text{O}_4/\text{TiO}_2/\text{SiO}_2$ nanocomposite is useful photocatalysts.

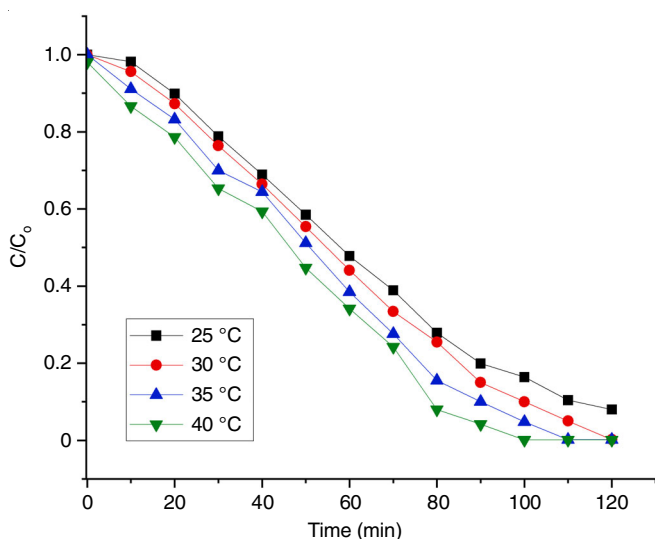


Fig. 9. Effect of temperature on $\text{MgFe}_2\text{O}_4/\text{TiO}_2/\text{SiO}_2$

Effect of catalyst dosage: To investigate the influence of nanocomposite concentration on the photocatalytic degradation of brilliant green dye, the dosage of produced nanocomposite was adjusted from 0.20 g/L to 0.50 g/L at pH of 8 and an initial brilliant green dye concentration of 10 mg/L. Fig. 10 demonstrates that the photocatalytic degradation rate of brilliant green

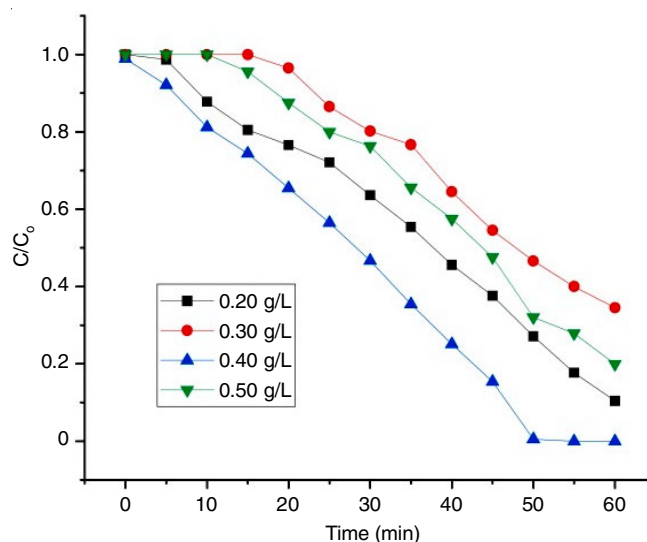


Fig. 10. Effect of catalyst dosage on $\text{MgFe}_2\text{O}_4/\text{TiO}_2/\text{SiO}_2$

escalated with higher composite loading, reaching a maximum at 0.40 g/L. The increased rate of deterioration can be attributable to the bigger overall surface area and/or the greater number of accessible active sites. However, as the composite loading continues to increase, the rate of degradation decreases, which can be explained by the dispersion of the catalyst and thereby reduces the availability of active sites for light absorption. Moreover, the higher turbidity of solution with increased loading further diminishes the light penetration.

Effect of irradiation time: To eliminate the possible influence of dye on evaluating the photocatalytic activity of the prepared material, the photodegradation experiments utilizing brilliant green dye, under solar radiation conditions, were also carried out. The absorbance of brilliant green solutions under visible light at various irradiation times is shown in Fig. 11. During the illumination time, the absorption peaks of brilliant green dye diminish and nearly vanish after 90 min. After 90 min of radiation, the percentage of degradation for brilliant green is 93.9%, 87.2% and 87.2%, respectively.

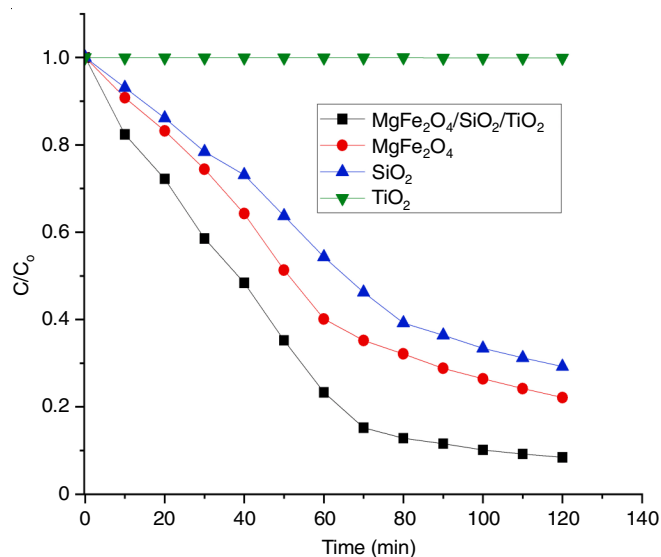


Fig. 11. Irradiation time on $\text{MgFe}_2\text{O}_4/\text{TiO}_2/\text{SiO}_2$

Reusability studies of photocatalyst: The stability and reusability of the photocatalyst, $\text{MgFe}_2\text{O}_4/\text{TiO}_2/\text{SiO}_2$, at the optimum load of 0.40 mg/L was also evaluated. An essential feature of the heterogeneous catalysis process that attracts industry is the reusability of catalyst. The process of reusing catalyst usually entails separating it from the reaction medium using filtration and/or centrifugation, followed by regeneration through washing with the appropriate liquids or heat treatment to eliminate surface intermediates which can cause deactivation or poisoning. In this work, the catalyst can be utilized again without needing to be washed with water or other liquids or separated from the reaction medium. The initial dye concentration of 10 ppm has been fixed by integrating the requisite amount of brilliant green into the colorless solution, so recovering the original concentration of 10 ppm. To perform recycling tests, the identical reaction conditions employed after the initial application were utilized to monitor the decrease in brilliant green concentration. According to the results (Fig. 12), the activity moderately declines (after 50 min, it drops from 98% in the first cycle to 93.4% and 75.9% in the second and third cycles, respectively).

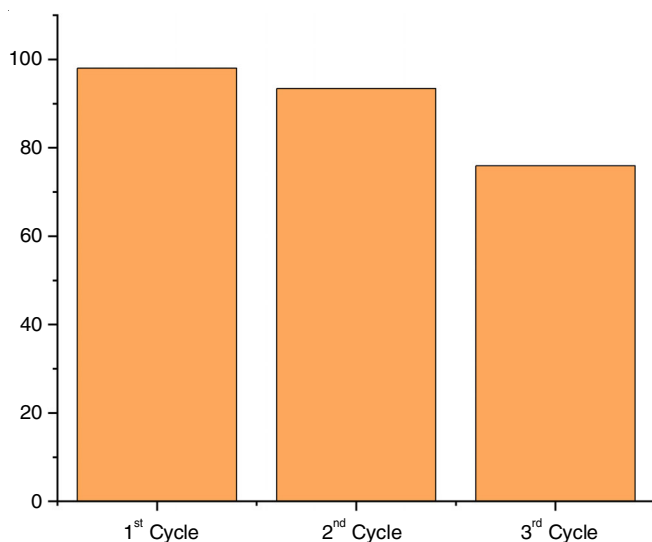


Fig. 12. Reusability of $\text{MgFe}_2\text{O}_4/\text{TiO}_2/\text{SiO}_2$

Antibacterial activity: The study results indicated that the synthesized nanocomposites also demonstrated promising antibacterial activity against *E. coli* (Gram-negative) and *S. aureus* (Gram-positive bacteria). Fig. 13 illustrates the antibacterial effect of $\text{MgFe}_2\text{O}_4/\text{TiO}_2/\text{SiO}_2$ mixed ternary metal oxide nanoparticles on *E. coli* and *S. aureus*. Zones of inhibition ranged from 15 mm to 14 mm at concentrations of 25 $\mu\text{g}/\text{mL}$. At concentrations of 100 $\mu\text{g}/\text{mL}$, the zones of inhibition measured 18 mm and 19 mm, respectively. These findings clearly show that the antibacterial activity of the synthesized nanocomposites was concentration-dependent and effectively inhibited the growth of pathogenic bacterial strains. The Gram-negative bacteria, with an outer membrane composed of negatively charged lipopolysaccharide molecules, likely allow the nano-materials to penetrate the bacterial cell wall, causing internal damage. The physical interaction between the bacterial cells

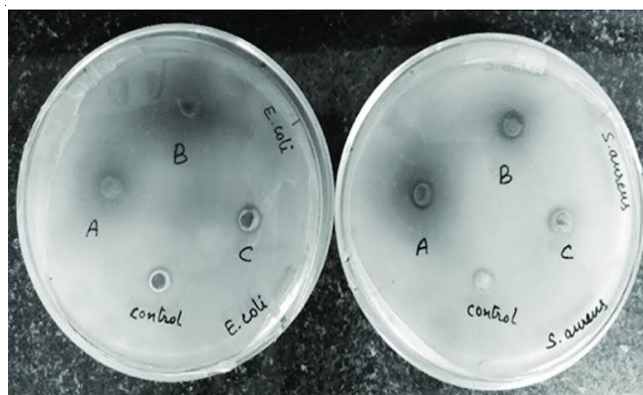


Fig. 13. Antibacterial activity of $\text{MgFe}_2\text{O}_4/\text{TiO}_2/\text{SiO}_2$

and the synthesized nanoparticles leads to cell wall disruption, eventually resulting in cell breakdown and bacterial death.

Conclusion

The work presents the effective nanocomposite magnetic photocatalyst $\text{MgFe}_2\text{O}_4/\text{TiO}_2/\text{SiO}_2$ nanocomposite was synthesized using the sol-gel method. Its photocatalytic activity was tested using brilliant green dye under UV-Vis light irradiation. The characterization results obtained through UV-DRS, XRD, FTIR, SEM, TEM and VSM indicate that $\text{MgFe}_2\text{O}_4/\text{TiO}_2/\text{SiO}_2$ is a good photocatalyst and a reusable, easily separable magnetic composite. A photocatalytic degradation process was optimized in terms of pH, catalyst dose, brilliant green concentration and catalyst reusability. The evaluation revealed greater degradation efficiency (100% in 125 min) at pH 8, 10 ppm brilliant green concentration, 0.40 g/L catalyst dosage and at least three-fold recyclability.

CONFLICT OF INTEREST

The authors declare that there is no conflict of interests regarding the publication of this article.

REFERENCES

1. A. Mittal, S. Sharma, T. Kumar, N.S. Chauhan, K. Kumari, S. Maken and N. Kumar, *J. Mater. Sci. Mater. Electron.*, **31**, 2010 (2020); <https://doi.org/10.1007/s10854-019-02720-z>
2. W. Somraksa, S. Suwanboon, P. Amornpitoksuk and C. Randorn, *Mater. Res.*, **23**, e20190627 (2020); <https://doi.org/10.1590/1980-5373-mr-2019-0627>
3. D. Bhattacharya, D. Ghoshal, D. Mondal, B.K. Paul, N. Bose, S. Das and M. Basu, *Results Phys.*, **12**, 1850 (2019); <https://doi.org/10.1016/j.rinp.2019.01.065>
4. M.A. Al-Nuaim, A.A. Alwasiti and Z.Y. Shnain, *Chem. Zvesti.*, **77**, 677 (2023); <https://doi.org/10.1007/s11696-022-02468-7>
5. M.B. Tahir, M. Sohaib, M. Sagir and M. Rafique, *Encyclopedia of Smart Mater.*, **2**, 578 (2022); <https://doi.org/10.1016/B978-0-12-815732-9.00006-1>
6. A. Tariq, U. Ullah, I. Ahmad, M. Asif, I. Sadiq and H. Haleem, *IET Nanobiotechnol.*, **13**, 697 (2019); <https://doi.org/10.1049/iet-nbt.2018.5032>
7. H.N.C. Dharma, J. Jaafar, N. Widiastuti, H. Matsuyama, S. Rajabsadeh, M.H.D. Othman, M.A. Rahman, N.N.M. Jafri, N.S. Suhaimin, A.M. Nasir and N.H. Alias, *Membranes*, **12**, 1 (2022); <https://doi.org/10.3390/membranes12030345>
8. R. Li, T. Li and Q. Zhou, *Catalysts*, **10**, 804 (2020); <https://doi.org/10.3390/catal10070804>

9. Y. Noratiqah and N.B. Ibrahim, *Appl. Phys., A Mater. Sci. Process.*, **129**, 1 (2023); <https://doi.org/10.1007/s00339-022-06289-z>
10. T. Tangcharoen, *Results Mater.*, **23**, 100596 (2024); <https://doi.org/10.1016/j.rinma.2024.100596>
11. V. Cappello, L. Marchetti, P. Parlanti, S. Landi, I. Tonazzini, M. Cecchini, V. Piazza and M. Gemmi, *Sci. Rep.*, **6**, 1 (2016); <https://doi.org/10.1038/s41598-016-0001-8>
12. A. Tariq, U. Ullah, I. Ahmad, M. Asif, I. Sadiq and H. Haleem, *IET Nanobiotechnol.*, **13**, 697 (2019); <https://doi.org/10.1049/iet-nbt.2018.5032>
13. R.L. Pozzo, M.A. Baltanas and A.E. Cassano, *Catal. Today*, **39**, 219 (1997); [https://doi.org/10.1016/S0920-5861\(97\)00103-X](https://doi.org/10.1016/S0920-5861(97)00103-X)
14. D. Beydoun, R. Amal, G. Low and S. McEvoy, *J. Mol. Catal. Chem.*, **180**, 193 (2001); [https://doi.org/10.1016/S1381-1169\(01\)00429-0](https://doi.org/10.1016/S1381-1169(01)00429-0)
15. H. Hamad, M. Abd El-Latif, A.E.-H. Kashyout, W. Sadik and M. Feteha, *New J. Chem.*, **39**, 3116 (2015); <https://doi.org/10.1039/C4NJ01821D>
16. N. Hosseinahli, M. Hasanov and M. Abbasi, *J. Water Reuse Desalin.*, **11**, 508 (2021); <https://doi.org/10.2166/wrd.2021.085>
17. S. Ryali and P.D. Sanasi, *J. Chin. Chem. Soc.*, **65**, 1423 (2018); <https://doi.org/10.1002/jccs.201800154>
18. J. Xue, H. Zhang, J. Zhao, X. Ou and Y. Ling, *J. Magnet. Magn. Mater.*, **514**, 167168 (2020); <https://doi.org/10.1016/j.jmmm.2020.167168>
19. G. Nagaraj, D. Brundha, C. Chandraleka, M. Arulpriya, V. Kowsalya, S. Sangavi, R. Jayalakshmi, S. Tamilarasu and R. Murugan, *SN Appl. Sci.*, **2**, 734 (2020); <https://doi.org/10.1007/s42452-020-2554-1>
20. O. Samuel, M.H.D. Othman, R. Kamaludin, O. Sinsamphanh, H. Abdullah, M.H. Puteh and T.A. Kurniawan, *Ceram. Int.*, **48**, 5845 (2020); <https://doi.org/10.1016/j.ceramint.2021.11.158>